Earth and Planetary Science Letters 583 (2022) 117445

Contents lists available at ScienceDirect

Earth and Planetary Science Letters

www.elsevier.com/locate/epsl

Northwest Pacific-Izanagi plate tectonics since Cretaceous times from western Pacific mantle structure

Jonny Wu [a,*], Yi-An Lin [a], Nicolas Flament [b], Jeremy Tsung-Jui Wu [a], Yiduo Liu [a]

[a] Department of Earth and Atmospheric Sciences, University of Houston, USA
[b] School of Earth and Environmental Sciences, University of Wollongong, Northfields Avenue, Wollongong, NSW 2522, Australia

ARTICLE INFO

Article history:
Received 25 October 2021
Accepted 16 February 2022
Available online xxxx
Editor: A. Webb

Keywords:
plate tectonics
seismic tomography
mantle structure
Panthalassa
western Pacific
East Asia

ABSTRACT

Northwest Pacific-Izanagi subduction histories along Eurasia are poorly constrained due to extensive subduction, which partially consumed the western Pacific plate and the entire Izanagi plate, its hypothesized conjugate margin. Here we reconstruct NW Pacific-Izanagi plate tectonics since Cretaceous times by mapping and structurally restoring (i.e. unfolding) the subducted western Pacific slabs from regional and global tomography, and re-creating the vanished Izanagi plate as its conjugate rift flank. Unfolding of the western Pacific slabs based on their cross-sectional areas, corrected for 'tomographic smearing', reveals that 2230 to 5000 km of western Pacific plate was subducted between Kamchatka and the southern Marianas. We add our restored western Pacific and Izanagi plates to a global plate model to reveal that Izanagi subduction under Eurasia after the mid-Cretaceous was limited between the present Bohai Bay-Yellow Sea, China, and northern Russia. The southern limit of Izanagi subduction was a NW-SE sinistral transform that intersected Eurasia near present Qingdao, China, and segmented eastern Eurasia continental magmatism during the late Cretaceous; we call this transform the 'Qingdao line'. We reconstruct a low-angle Izanagi-Pacific ridge-trench intersection with Eurasia at ~50 ± 10 Ma between Bohai Bay-Yellow Sea and northern Russia. The ~50 Ma Pacific plate motion change initiated subduction along the Qingdao line transform, forming the Izu-Bonin-Marianas arcs and reorganizing the Bohai Bay-Yellow Sea faults. We show tomographic and geodynamic modeling evidence that a 4000 km-long, laterally-continuous, NE-SW trending, seismically-slow 'slab gap' at 1000 ± 250 km depth between present northern Sakhalin and central China is the tomographic signature of the subducted Izanagi-Pacific ridge.

1. Introduction

Seafloor magnetic lineations within the northwest Pacific Ocean are oriented NE-SW and present seafloor ages that decrease northwestwards towards the western Pacific subduction zones (Fig. 1a) (e.g. Nakanishi et al., 1989). Based on plate tectonics theory, these seafloor age patterns imply significant subduction of the western Pacific plate younger than ~100 Myr and its entire conjugate rift flank, the conceptual Izanagi plate (e.g. Woods and Davies, 1982; Engebretson et al., 1985; Müller et al., 2016). As a result, plate tectonic reconstructions since Cretaceous times for a >8000 km-long swath of the northwest Pacific margin between SE Asia and northern Russia remain poorly established (Figs. 1b to d) (e.g. Maruyama et al., 1997; Li et al., 2014; Seton et al., 2015; Domeier et al., 2017).

Pacific-Panthalassan plate tectonic reconstructions are recognized as the most challenging areas to reconstruct on Earth since the Mesozoic due to extensive subduction along eastern Eurasia (>6000 km since the late Cretaceous) (Müller et al., 2016; Torsvik et al., 2019). These uncertainties create plate reconstruction knowledge gaps for 65% of oceanic areas (up to 45% of Earth's surface) during Cenozoic and Mesozoic times (Torsvik et al., 2019) that hamper our understanding of past global atmospheric CO_2 (Van Der Meer et al., 2014), true polar wander (Mitchell et al., 2021), and supercontinent evolution (Li et al., 2019c), since Panthalassa was the superocean that surrounded Pangea during early Mesozoic times. Here we use an unfolded-slab plate tectonic method (Wu et al., 2016) with a new update for mitigating tomographic image degradation to reconstruct northwest Pacific and Izanagi plate tectonic model from western Pacific mantle structure. We show our plate model is consistent with relatively independent East Asian regional geology and geochemistry. We compare our mapped mantle structure to an updated, previously-published geodynamic model and show a possible Izanagi-Pacific ridge subduction tomographic signature under East Asia. Our identified subduction realms within NW Pacific-Panthalassa during Cretaceous times newly define adjacent subduction domains (i.e. Kula, Junction, and the east-

* Corresponding author.
E-mail address: jwu40@central.uh.edu (J. Wu).

https://doi.org/10.1016/j.epsl.2022.117445

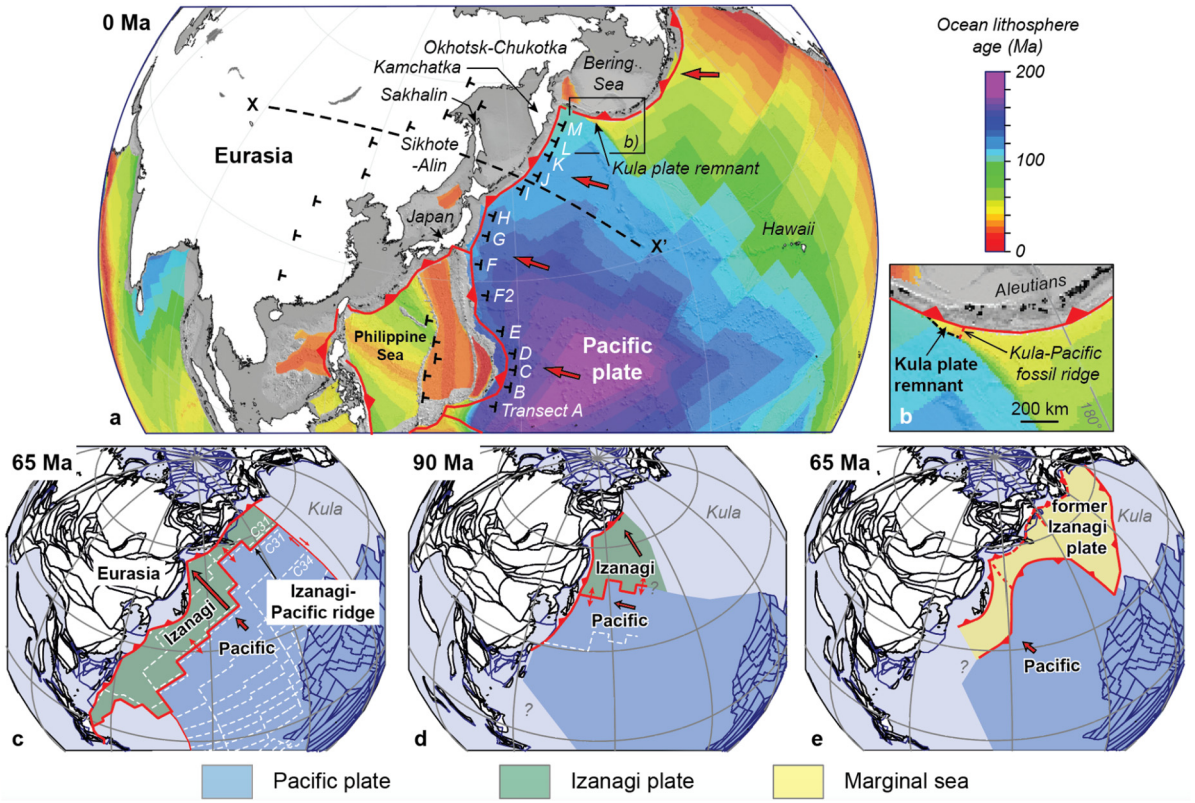

Fig. 1. a) Plate tectonic setting of the northwest part of the Pacific plate, northeast Eurasia, and surrounding areas. Rainbow colors indicate seafloor ages from Müller et al. (2016). Dashed black line shows the location of profile X-X' in Fig. 2. Black T-shaped markers show location of tomographic transects A to M in this study (detailed locations are shown in Fig. S3). Red arrows show present Pacific plate motion. b) Inset map showing Kula plate remnant and Kula-Pacific fossil ridge south of the Bering Sea and Aleutian subduction zone (after Lonsdale, 1998). c) to e) Highly contrasted plate reconstructions of the northwest Pacific plate (blue), the Izanagi plate (green) and former marginal seas (yellow) have been proposed that can be differentiated by their implied ridge-trench intersections along Eurasia. In c) the Izanagi-Pacific spreading ridge subducted sub-parallel to the Eurasian margin in the early Cenozoic, based in part on >4000 km of 'synthetic seafloor isochrons' (white dashed lines) that extend from the existing Pacific plate (dark blue polygons to the southeast) (after Whittaker et al., 2007; Seton et al., 2015; Müller et al., 2016). d) A spreading ridge subducted at a high angle near Japan in the late Cretaceous that was the Izanagi-Pacific ridge (simplified from Maruyama et al., 1997), the Kula-Pacific ridge (Uyeda and Miyashiro, 1974), or a former marginal sea spreading ridge (Itoh et al., 2017). e) The Izanagi-Pacific spreading ridge inverted in the Cretaceous and formed a south-dipping intra-oceanic subduction zone (Domeier et al., 2017) that precluded Izanagi-Pacific ridge-trench intersection with Eurasia. Larger red arrows show Pacific and Izanagi plate motion directions. (For interpretation of the colors in the figure(s), the reader is referred to the web version of this article.)

ern Tethys) and reveal details of the western Pacific-Panthalassan superocean during supercontinent break-up.

1.1. Review of northwest Pacific-Izanagi plate tectonic reconstructions

Published northwest Pacific-Izanagi plate models differ on reconstructed Izanagi and Pacific plate geometries, the existence of marginal seas and other oceanic plates along Eurasia, and imply contrasted spatio-temporal Izanagi-Pacific ridge-trench intersections with Eurasia (Fig. 1c-e). One class of models reconstructs a low-angle Izanagi-Pacific ridge-trench intersection with eastern Eurasia during early Cenozoic times (Fig. 1c) (Whittaker et al., 2007; Seton et al., 2015). The ridge-trench intersection was preceded by Izanagi subduction and followed by Pacific subduction afterwards (Fig. 1c). This model assumes the Izanagi-Pacific spreading ridge was active until its subduction (Fig. 1c) (Whittaker et al., 2007; Seton et al., 2015). The early Cenozoic low-angle ridge-trench intersection is supported by a widespread 56 Ma to 46 Ma NE Asian continental arc magmatic hiatus, igneous rock isotopic changes from enriched to depleted signatures that are consistent with mantle flow through a slab window, intrusion of mid-ocean ridge basaltic (MORB) intrusions into unconsolidated forearc sediments, high heat flow, and uplift between Japan and the Russian Far East (Kimura et al., 2019; Wu and Wu, 2019). Within this region, the Hidaka magmatic zone, Hokkaido, Japan, shows evidence for a slightly younger ridge-trench intersection at 46 to 37 Ma, potentially due to subduction of an offset ridge-transform segment (Yamasaki et al., 2021). However, it is currently debated whether the low-angle Izanagi-Pacific ridge-trench intersection was extensive (i.e. stretched from SE Asia to Alaska) (Fig. 1c) (Whittaker et al., 2007; Seton et al., 2015) or was limited to regions north of SW Japan (Wu and Wu, 2019) and south of Sakhalin (Vaes et al., 2019). Some studies dispute the early Cenozoic ridge-trench intersection and prefer to interpret the geology in terms of stalled subduction, reorganization into a transform margin, followed by slab break-off (e.g. Grebennikov et al., 2021).

Other plate models assume the Izanagi-Pacific ridge ceased spreading by mid- to late-Cretaceous times (Fig. 1d) (Engebretson et al., 1985; Maruyama et al., 1997). These models reconstruct a high-angle Izanagi-Pacific ridge-trench intersection along eastern Eurasia during the Late Cretaceous that places the Pacific plate south of Japan and the Izanagi plate north of Japan (Fig. 1d). The predicted ridge-trench intersection is consistent with high heat flow and rapid exhumation of the Sanbagawa metamorphic belt, Japan, during late Cretaceous times (Maruyama et al., 1997). Adakites and extensive copper-gold deposits near Shanghai, China (e.g. Li et al., 2014) and adakitic Kitakami granitic plutons at NE Japan (Osozawa et al., 2019) formed during Early Cretaceous times have also been explained by this model.

Marginal seas along Eurasia during Cretaceous or early Cenozoic times have been reconstructed based on accreted, far-traveled, allochthonous oceanic arc remnants (Fig. 1e) (e.g. Konstantinovskaia, 2001; Ueda and Miyashita, 2005; Domeier et al., 2017; Yamasaki

and Nanayama, 2018; Vaes et al., 2019; Kutyrev et al., 2021). It is now generally agreed that now-vanished marginal seas once existed within the north Pacific basin (i.e. Kamchatka and surrounding areas) during late Cretaceous to mid-Cenozoic times (Konstantinovskaia, 2001; Domeier et al., 2017; Vaes et al., 2019). This is supported by an abrupt termination of continental arc magmatism along the Okhotsk-Chukotka margin north of Kamchatka at ~78 to 76 Ma, which has been attributed to a shift of the subduction zone towards the offshore (Akinin and Miller, 2011). However, the tectonic reconstruction of marginal seas south of Kamchatka, including Japan and Sikhote-Alin (Ueda and Miyashita, 2005; Itoh et al., 2017) and southeast China (Fig. 1c to e) (e.g. Müller et al., 2016; Wu et al., 2016), remain debated.

The preserved 'Kula' plate remnant offshore the Aleutians (Fig. 1b) adds further complexities to NW Pacific plate reconstructions because it implies an oceanic 'Kula plate' also existed within the north Pacific basin during the Mesozoic and Cenozoic eras (Woods and Davies, 1982; Lonsdale, 1988). Although the Kula plate has mostly subducted (Fig. 1b), it may have been extensive and subducted along northeast Asia during Cretaceous or early Cenozoic times (Engebretson et al., 1985; Lewis et al., 2002). Other studies proposed that the Kula plate was spatially limited to areas east of northern Russia and never subducted along East Asia (Fig. 1c,e) (e.g. Konstantinovskaia, 2001; Müller et al., 2016; Domeier et al., 2017; Vaes et al., 2019).

2. Data and methods

2.1. Tomography

We identify subducted western Pacific oceanic lithosphere from two primary tomographic models: (1) the global P-wave tomography MITP08 (Li et al., 2008); and, (2) the regional, full-waveform tomography FWEA18 P- and S-wave models, which cover a more limited area (~32°N to 47°N) along eastern Eurasia (Tao et al., 2018). To mitigate bias, we compare our results against selected suites of published P- and S-wave global tomographic models (Supplemental Text S1). We do not use tomographic vote maps despite their advantages (Shephard et al., 2017) because some tomographic models specifically access regional East Asian seismological records.

2.2. 3D slab mapping and unfolding

We map slabs in three-dimensions using the software GOCAD following Wu et al. (2016). Slabs were mapped from the following criteria: faster-than-average seismic velocity perturbations (0.2-1% and >1% faster in global and regional tomography, respectively), Benioff zone seismicity, and steep velocity gradients at the anomaly edges (i.e. clustering of velocity perturbation contour lines). To create a 3D mid-slab map (e.g. Animation 1), we consider the center of the slab anomaly (i.e. mid-slab) as the most probable slab location and select 2D mid-slab curves along hundreds of variably-oriented tomographic transects (e.g. Fig. S1) to form a triangulated mid-slab surface. Tomographic velocities are extracted along the mid-slab surface nodes to analyze intra-slab velocity variations (e.g. Animation 1). The 3D mid-slab map enables us to maintain a spatially self-consistent slab model to guide the slab unfolding, described next.

Slab unfolding The amount of subducted western Pacific oceanic lithosphere is quantified following the 'cross-sectional slab area unfolding' method of Wu et al. (2016) (Fig. 2) with an update to address artificial expansion of slab volumes from tomographic imaging (Fig. 2c). In this method, the pre-subduction length of the subducted oceanic lithosphere is structurally restored (i.e. unfolded) using area conservation and an assumed initial oceanic lithospheric thickness (Fig. 2). We first select the slab area from a spherical Earth-projected tomographic cross-section (dashed white lines showing the slab edges in Fig. 2a). Our slab edge selections are necessarily interpretive and we mitigate bias by using two different criteria: 1) we manually interpret a primary set of slab edges by following the most closely-spaced velocity perturbation contours that close around a slab anomaly (i.e. stronger velocity gradients); and 2) we compute an alternative set of 'machine-guided' slab edges from velocity isocontours. A small number of shallow (<400 km depth) fast anomalies that are unlikely to be slabs based on previous studies are manually excluded (e.g. 'Ordos block' in Fig. 2a; Li et al., 2008). We then structurally restore (i.e. unfolded) the selected slab area to Earth's surface (Fig. 2b), correcting for density-depth changes within the mantle following PREM (Dziewonski and Anderson, 1981) as in Wu et al. (2016). Our unfolding assumes a 75 km initial oceanic lithospheric thickness (Fig. 2b) based on Mesozoic western Pacific seafloor ages (Fig. 1a) and RHCW18 'plate model' thermal structure (Richards et al., 2018). We check our assumed thickness against the implied oceanic lithospheric thicknesses from our final plate model and briefly discuss uncertainties in 3.2.

We improve the method of Wu et al. (2016) by adding a correction for the artificial expansion of tomographically-imaged slab areas due to blurring, or 'tomographic smearing' (e.g. Simmons et al., 2019). We base our 'tomographic smearing correction' on the difference between input and output slab areas from nearby synthetic slab resolution tests (Fig. 2c). Although such tests offer optimistic views on resolution, they provide some measure of imaging artifacts on our slab unfolding. We analyze the three available MITP08 resolution tests within the local area (Li, 2007). We find that after inversion, the output Pacific slab areas expanded by an average of ~25% (maximum 41%; minimum 12%) (Fig. S4). Ideally, a spatially-varying correction would be applied but do not have sufficient resolution tests. Therefore, we take a pragmatic approach to examine the range of possibility by considering three cases: a 'mean' case tomographic smearing correction of 25% (i.e. we reduce our cross-sectional slab areas from global tomography by 25%) (Fig. 2d); and 'minimum' and 'maximum' tomographic smearing correction cases of 10% and 40%, respectively. We do not apply a tomographic smearing correction to the regional, full-waveform tomography FWEA18 because point spread resolution tests show only relatively minor smearing at depths of interest (i.e. above 900 km) and the imaged slabs show relatively narrower and higher velocity perturbation anomalies (3.5 to 5% perturbations compared to 1%) compared to global tomography (e.g. Figs. S2, S3) (Tao et al., 2018).

Unfolded-slab plate tectonic modeling We build a quantitative 'unfolded-slab plate tectonic model' by adding our unfolded Pacific slabs to a seafloor spreading-based, global plate reconstruction with corrected Pacific-Panthalassa angular velocities (i.e. Earthbyte Model R) (Matthews et al., 2016; Torsvik et al., 2019). Plate kinematics are developed by attaching unfolded slab lengths to their present-day subduction zones and assigning the associated plate motions within the software GPlates. We reconstruct our unfolded slabs as straight lines and not kinked (e.g. Fuston and Wu, 2020; Parsons et al., 2021) because our final model reconstructs subduction of the western Pacific slabs under Eurasia after ~50 Ma; during this period Pacific plate motions were westwards and relatively stable. We impose synthetic seafloor isochrons on the unfolded western Pacific slabs and reconstruct the Izanagi plate as its conjugate margin assuming symmetric spreading (Fig. S7). Asymmetric spreading is possible but our assumed symmetric spreading is most straightforward and accounts for >90% of Earth's seafloor spreading within our reconstruction time period (e.g. Müller et al., 2016).

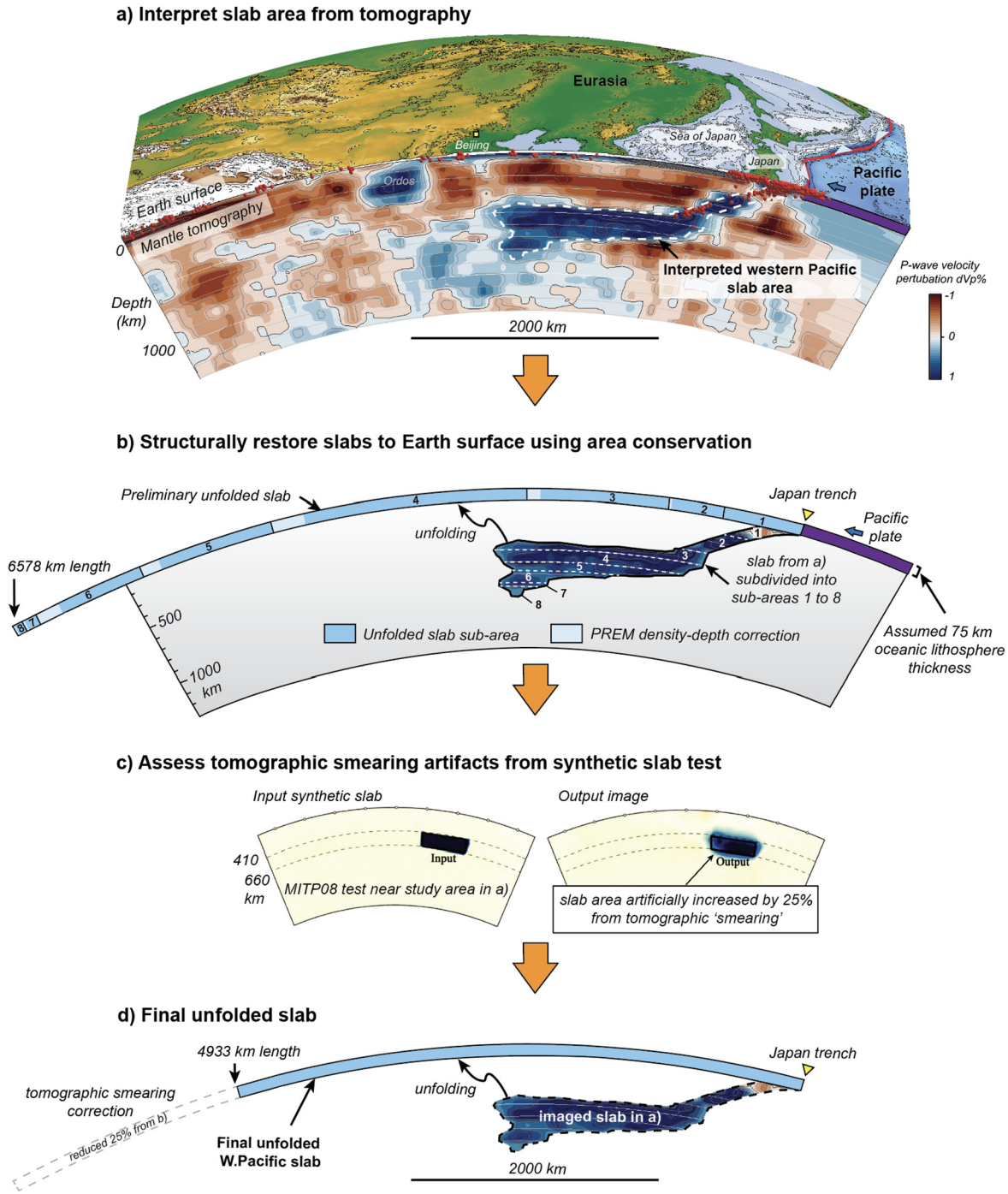

Fig. 2. Example of the cross-sectional slab area unfolding method to estimate the pre-subduction length of a subducted slab from tomography. a) 3D view of MITP08 tomography (Li et al., 2008) and Earth surface. The slab area (white dashed line) is interpreted from tomographic velocity iso-contours and by considering stronger velocity gradients to be indicative of slab edges. b) The slab is sub-divided into sub-areas by depth and structurally restored to Earth's surface using area conservation and an assumed lithospheric thickness (75 km in this example). A density-depth correction (lighter blue areas) is applied following PREM (Dziewonski and Anderson, 1981). An initial unfolded slab length of 6578 km is computed. c) Cross-sectional slab areas from input and output synthetic slab tests are compared to estimate the amount of tomographic smearing (i.e. artificial increase of slab areas due to image blurring), which in this case was found to be ~25%. d) The unfolded slab lengths from b) are corrected for tomographic smearing (i.e. reduced by 25%) and a final unfolded western Pacific slab length is estimated at ~4930 km.

3. Results

3.1. Western Pacific 3D mid-slab map

We map a western Pacific mid-slab surface between Kamchatka (55°N) and near-equatorial latitudes from seismicity and MITP08 tomography (Fig. 3a). Our mapped slabs follow relatively faster velocity anomalies that show seismicity and extend downwards from the modern western Pacific trenches (Figs. 3c, S1; Animation 1). Our extracted tomographic velocities along our western Pacific mid-slab generally shows fast velocities (Fig. 3b) with the exception of a slower velocity 'slab gap' under NE China, which has been noted in other tomographic studies (e.g. Tang et al., 2014; Tao et al., 2018). The northernmost region along Kurile-Kamchatka shows a swath of deeper subducted slabs down to ~900 km depths (Figs. 3a, c). The northern edge of that slab abruptly terminates

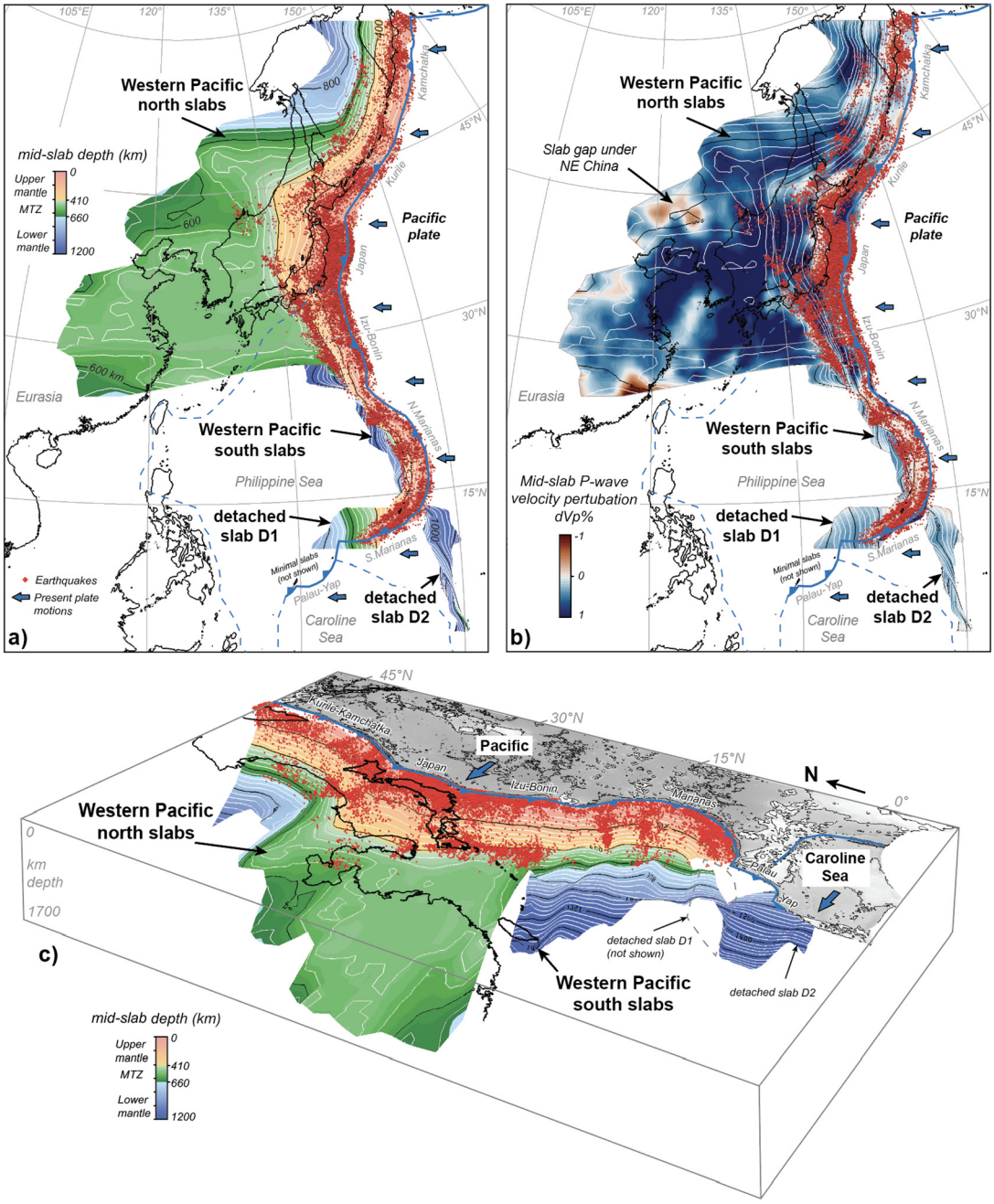

Fig. 3. Maps of the subducting western Pacific slabs showing a) mid-slab depths and b) extracted mid-slab P-wave tomographic velocities. c) 3D visualization of a). The slabs were mapped from MITP08 global tomography and earthquakes (red dots). Contour lines show the mid-slab depths at 200 km intervals (black lines) and 40 km intervals (white lines). The western Pacific slabs lie sub-horizontally below eastern Eurasia north of 28°N within the upper mantle and mantle transition zone (MTZ). In contrast, the Pacific slabs are sub-vertical south of 28°N. Two swaths of deeper, detached slabs were mapped near the southern Marianas and under the present Pacific plate south of the central Marianas trench. See also the 3D movie of the mid-slab model (Animation 1) and tomographic cross-sections showing the interpreted mid-slab surface (Fig. S1).

around 55°N along Kamchatka (Fig. 3a, c). Continuing south to 28°N, the western Pacific slabs extend westwards and lie sub-horizontally within the mantle transition zone (i.e. 410 to 660 km depths) under China, Korea and Japan (Fig. 3a, c). The slab structure abruptly changes from sub-horizontal north of 28°N to sub-vertical south of 28°N (Fig. 3a). This first-order structural feature has been well-documented in previous studies (e.g. van der Hilst and Seno, 1993). South of 28°N, the sub-vertical western Pacific slabs strike SSE and extend down to ~1100 km depths (Fig. 3a, Animation 1). We also map two swaths of detached slabs D1 and D2 near the southern Marianas and south of the central Marianas (Fig. 3a, Animation 1). The detached slabs D1 and D2 are seen in other tomographic models (Miller et al., 2006; Jaxybulatov et al., 2013) and do not appear very well-resolved based on their lower P-wave perturbations and weaker gradients compared to northern areas (e.g. Fig. S1m,n). Overall, our mapped western Pacific slab geometries are generally consistent with previous tomographic studies (e.g. van der Hilst and Seno, 1993; Miller et al., 2006; Jaxybulatov et al., 2013) and provide a comprehensive 3D view of both seismic and aseismic subducted slabs along the western Pacific (Animation 1).

3.2. Western Pacific slab unfolding

We interpret western Pacific cross-sectional slab areas along 14 MITP18 tomographic transects between 11°N to 53°N latitudes

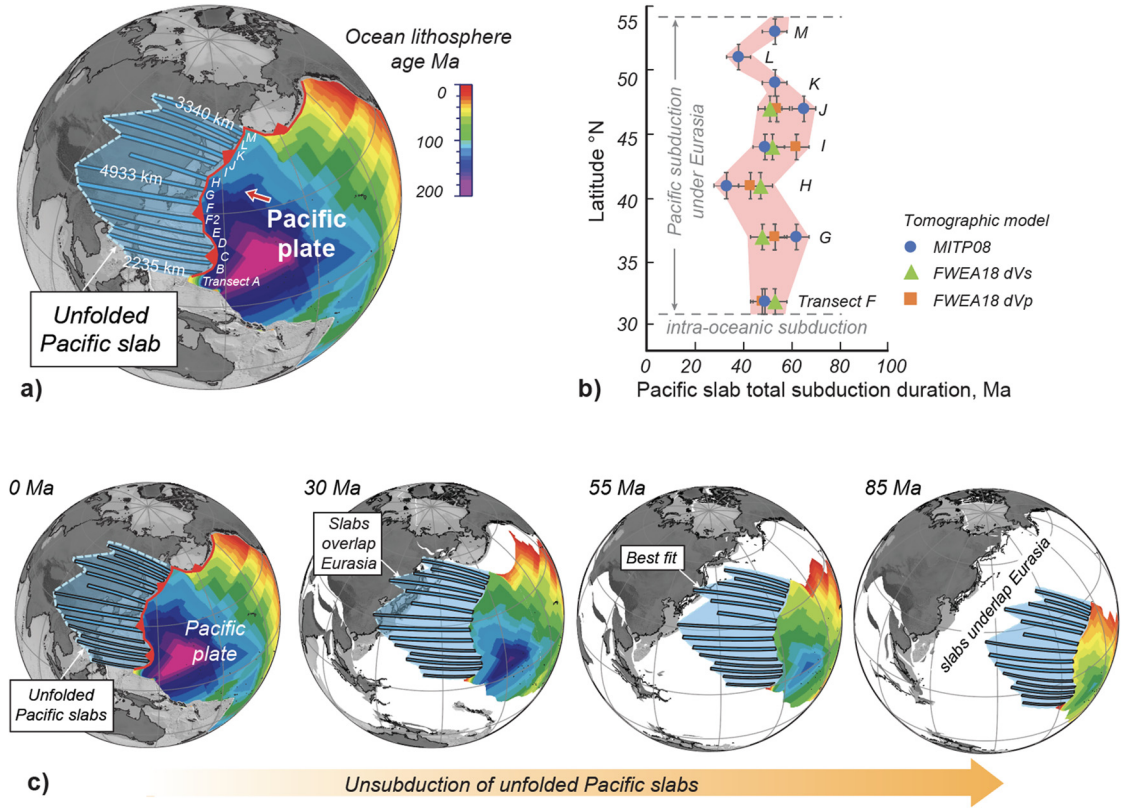

Fig. 4. Western Pacific slab unfolding from tomography. a) Unfolded Pacific slab lengths from MITP08 tomography for transects A to M (see also Table S1). Blue bars show the Pacific slab unfolded lengths. The transparent blue polygon in a) shows the implied pre-subduction size of the western Pacific slabs based on our unfolding. Rainbow colors show seafloor ages within the existing Pacific plate. b) Total subduction duration for the unfolded Pacific slabs based on Eurasia-Pacific convergence from a global tectonic reconstruction (Müller et al., 2016). Our slab unfolding implies the Pacific slabs began to subduct along the Eurasian margin at ~50 ± 10 Ma, as highlighted by the transparent red fill. c) Progressive unsubduction of our unfolded western Pacific slabs by attaching the unfolded slabs to the existing Pacific and reversing Pacific and Eurasia plate motions from the global plate model. Our unfolded Pacific slabs best account for lost oceanic lithosphere back to ~55 Ma based on minimal overlap between the unfolded Pacific slabs and reconstructed Eurasia.

(Figs. S2) and five FWEA18 transects between ~30°N to 49°N latitudes (Fig. S3). All transects were roughly oriented along the present Pacific plate convergence direction (Fig. 1a). Our slab unfolding from MITP08 global tomography between 11°N to 53°N corrected for 'mean case' 25% tomographic smearing (see Methods in 2.2) reveals pre-subduction western Pacific slab lengths between 2235 km and 4933 km (Fig. 4a, Table S1). Our Pacific slabs from FWEA18 P- and S-wave tomography show unfolded slab lengths of ~3500 km and 5200 km within its area of coverage 32°N to 47°N (Table S1). The lengths are generally comparable to the 'mean case' smearing-corrected MITP08 unfolded slab lengths within the same area (3000 km and 4900 km) (Table S1); further comparisons are made below. We display our MITP08 unfolded slab lengths with the existing Pacific plate to show the pre-subducted size of the western Pacific plate (Fig. 4a). We do not implement the shorter length along Transect H in our unfolded western Pacific slab boundary (blue dashed line in Fig. 4a) because it occurs along the interpreted slab 'hole' above a possible mantle upwelling under NE China (Figs. 2b; S1 to S3) (Tang et al., 2014), which may have distorted or partially destroyed the slabs (i.e. reduced slab areas).

Comparison to slab unfolding from other tomography and alternative slab edges We compare our western Pacific slab unfolding (Fig. 4b) to other global tomography along Transects F to J (Fig. 1), which is the area of common coverage for all five tomography used in this study (MITP08, UUP07, GAPP4, FWEA18 S-wave, FWEA18 P-wave; see Text S1 for more information). We estimate unfolded slab lengths from both manually-selected and computer-generated slab edges (i.e. isovalues) for the three global tomography (Fig. S6; Tables S2 and S3). We do not calculate isovalue slab edges for FWEA18 because it was unavailable at this stage of the study. In total, eight unfolded slab lengths are produced per transect. We find the unfolded slab lengths from all estimates generally plot within the range of our 10% minimum to 40% maximum tomographic smearing correction cases from MITP08 (yellow area in Fig. S6a). Therefore, we will later account for uncertainties from the various tomographic model and selected slab edges by considering our minimum and maximum cases within the plate tectonic model (Figs. S6b to d).

Uncertainty from assumed pre-subduction lithospheric thickness We test our assumed 75 km pre-subduction ocean lithospheric thickness for slab unfolding (Fig. 2b) along a central Transect G by comparing against the lithospheric thicknesses implied by the seafloor isochrons our final plate model (Fig. 5). Estimates of oceanic lithospheric thicknesses from its age are an active research area; nonetheless, we compute lithospheric thicknesses from age using the 1175 °C isotherm from the RHCW18 plate model, which fits with the lithosphere-asthenosphere boundary from azimuthal anisotropy studies (Richards et al., 2018). Our final plate model implies the subducted Pacific slabs had an average thickness of 86 km, which is 14% thicker than our assumed constant 75 km thickness (Table S4). We re-compute our slab unfolding using a 14% thicker pre-subduction lithosphere thickness and find the unfolded slab length is shorter than our mean case but within the range of our minimum and maximum cases (red diamond in Fig. S6). This suggests that lithospheric thickness uncertainties can be adequately captured by our minimum and maximum cases (Figs. S6b to d), with minor preference for the maximum case (i.e. shorter slab lengths in Fig. S6d) over the minimum case.

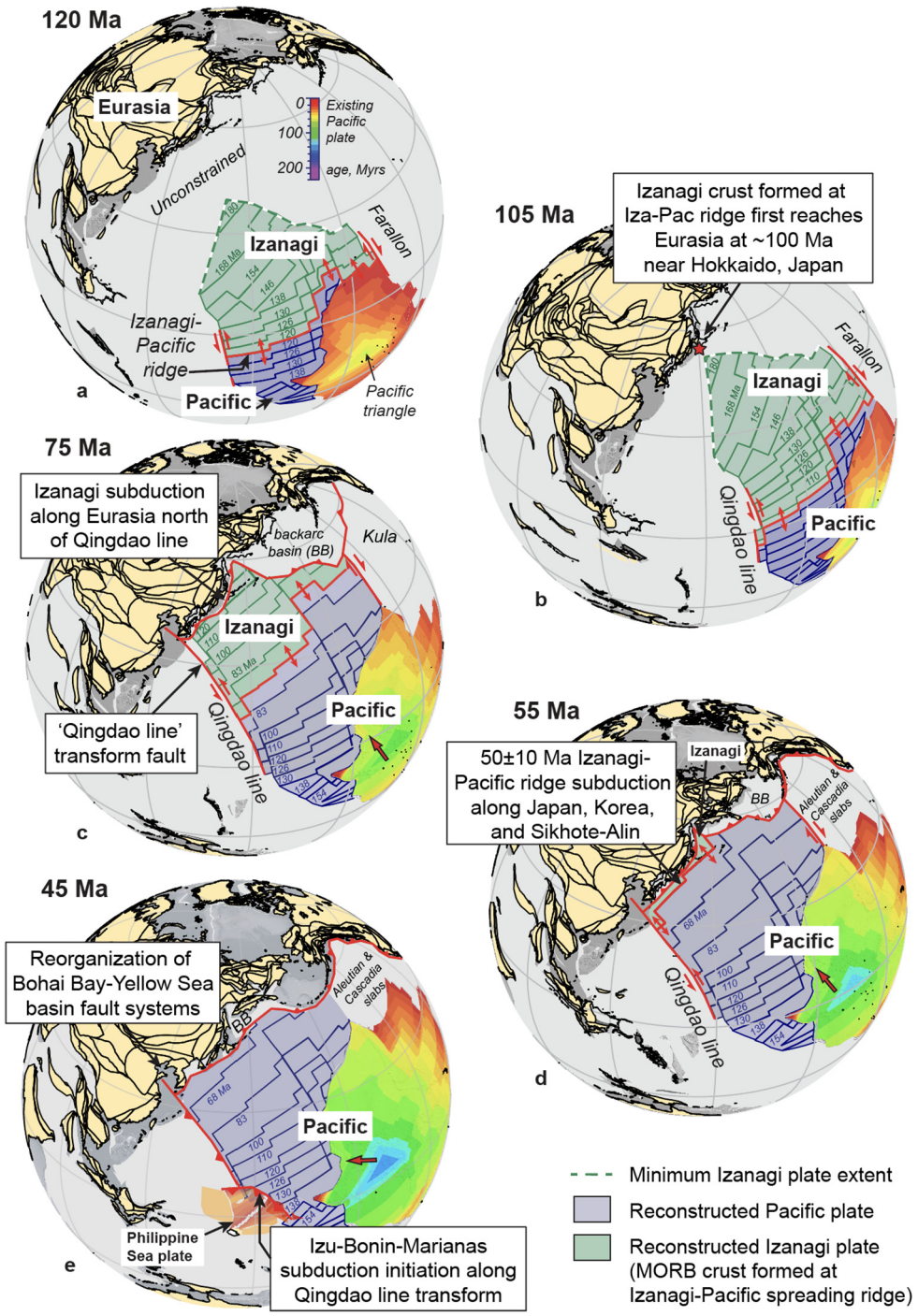

Fig. 5. Northwest Pacific-Izanagi unfolded-slab plate reconstruction from this study. The Pacific plate was restored by unfolding the western Pacific slabs, whereas the Izanagi plate was modeled as its conjugate rift flank. Symmetric seafloor spreading is assumed. The restored plates were added to the Earthbyte model 'R' with corrected Pacific-Panthalassa angular velocities (Matthews et al., 2016; Torsvik et al., 2019). Our resultant 'unfolded-slab' plate model implies: (1) Izanagi subduction was limited to the region between westernmost Alaska and Korea; thus, the Izanagi plate never subducted under southeast China; (2) the Izanagi plate reached the East Asian margin near Sikhote-Alin by latest mid-Cretaceous times (~105 Ma and possibly earlier), and was completely subducted by 50 Ma; (3) the Izanagi-Pacific spreading ridge intersected the East Asian margin at a low angle at 50 ± 10 Ma between Korea and northern Russia. Ridge subduction did not occur south of Korea. The southwest Izanagi-Pacific realm was bounded by a transform fault that intersected Eurasia near present Qingdao, China, that we call the 'Qingdao line'. After 50 Ma, subduction initiated along the Qingdao line transform and produced the Izu-Bonin-Marianas intra-oceanic arcs.

3.3. Western Pacific total subduction duration from slab unfolding

Following Wu et al. (2016), we estimate Pacific slab subduction duration by comparing our unfolded slab lengths to Pacific-Eurasia plate convergence history from a global plate model (Fig. S5). We do not compute Pacific slab subduction durations for areas south of ~32°N because they require reconstructed marginal sea motions (i.e. Philippine Sea plate or other vanished plates), which are controversial. North of 32°N (i.e. Japan, Kuril and Kamchatka trenches), our mean case implies the western Pacific slabs began to subduct along Eurasia at ~50 ± 10 Ma (red area in Fig. 4b). We reverse Pacific plate motions and attach the unfolded Pacific slabs within the global plate model to show this graphically (Fig. 4c). Moving backwards in time, the leading edge of our reconstructed western Pa-

cific plate fits best (i.e. minimal overlap) with the eastern Eurasian margin around 55 Ma (Fig. 4c). Comparison to our minimum and maximum cases indicate a wider time range ~40 to ~70 Ma, or 55±15 Ma (Fig. S6b to d). Although we did not compute Pacific slab subduction durations for areas south of 32°N due to probable intra-oceanic subduction, we note our final plate model generates a ~50 Ma Pacific subduction duration along the Izu-Bonin-Marianas (IBM) (Figs. 5d,e), which is consistent with well-known IBM subduction initiation (Li et al., 2019a).

Comparison to previous slab unfolding studies Previous studies estimate a total subduction duration of 30 to 25 Ma for the subducted western Pacific slabs along Japan (Liu et al., 2017; Tao et al., 2018), which is significantly younger than our 50 ± 10 Ma mean case estimate (Fig. 4b) and outside of our minimum/maximum cases (i.e. 55±15 Ma) (Figs. S6b to d). Although a minor source of discrepancy could be our inclusion of smaller slab fragments near the Pacific slab leading edge (Figs. S2, S3), the main reason for the differences stems from the respective slab unfolding methods. The previous studies measure the amount of subducted slab from its 'line length' and assume that slabs do not thicken after subduction (Liu et al., 2017; Tao et al., 2018). In contrast, our method will estimate longer slab lengths because it considers the slab cross-sectional area (Fig. 2). This approach allows for post-subduction slab thickening due to slab buckling and thickening, which is seen in geodynamic models (e.g. Čížková and Bina, 2013). Therefore, we consider the previous studies indicate a minimum subduction duration for the Pacific slabs.

3.4. Tectonic significance of the reconstructed western Pacific plate leading edge

Our results imply the western Pacific plate leading edge intersected eastern Eurasia around 50 ± 10 Ma along Korea, Japan and the Russian Far East (Fig. 4b,c), with a wider range of possibility between 40 and 70 Ma (Fig. S6b to d). Within this time window, our results show a spatiotemporal match to the widespread 56 to 46 Ma Pacific-Izanagi ridge-trench intersection along Eurasia between Japan to Sikhote-Alin, Russian Far East (Wu and Wu, 2019; Kimura et al., 2019). Whittaker et al. (2007) also independently reconstructed the missing western Pacific plate from synthetic seafloor isochrons and concluded the Izanagi-Pacific spreading ridge intersected the Eurasian margin between ~60 Ma to 50 Ma (e.g. Fig. 1a). Therefore, we interpret the Izanagi-Pacific spreading ridge was located at the leading edge of our reconstructed Pacific plate. We proceed to build our tomography-led plate model using this inference and will further compare our model against a wider swath of geological and geophysical evidence in Section 4.

3.5. Unfolded-slab plate reconstruction of the NW Pacific-Izanagi plates

We reconstruct past plate kinematics by imposing a map of past ages of the Pacific Ocean on our unfolded Pacific slabs using the software GPlates (Figs. 5 and S7) (Müller et al., 2018). As mentioned in 3.4, the synthetic seafloor isochrons of Whittaker et al. (2007) are generally compatible with our slab unfolding. Therefore, we use an updated version of the Whittaker et al. (2007) Pacific synthetic seafloor isochrons (Müller et al., 2016) but only impose these isochrons within the limits of our unfolded western Pacific slab only (Fig. S7a,b). Our adapted synthetic seafloor isochrons includes two areas (A and B in Fig. S7b) that are not directly supported by our slab unfolding but are plausible. In Area A we reconstruct additional ocean lithosphere within the north Pacific to maintain a NW-younging ocean basin seafloor age progression (Fig. S7b) even though we did not find slabs under Eurasia to directly support this inference. The Area A lithosphere may have subducted along northern Pacific backarc basins during the Late Cretaceous to Eocene (e.g. Domeier et al., 2017; Vaes et al., 2019) or could have been captured to form the Bering Sea, which has an unknown origin (Cooper et al., 1976). We mapped slabs within Area B (detached slab D2 in Fig. 3a) but they were not unfolded due to tomographic resolution and Caroline Sea plate reconstruction uncertainties; thus, we inferred the Area B lithosphere based on the minimum extent of the eastern Pacific triangle.

We reconstruct the Izanagi plate and its seafloor isochrons by assuming a conjugate rift flank and symmetric spreading from the western Pacific plate (Fig. S7c). This results in a fully-reconstructed Pacific-Izanagi ocean basin age sequence formed by the existing Pacific plate, our unfolded western Pacific slabs, and an Izanagi conjugate rift flank (Fig. S7c). We add our restored Izanagi and Pacific plates into a global plate model (Matthews et al., 2016) with Pacific-Panthalassa corrections (Model R; Torsvik et al., 2019) to create an unfolded-slab Izanagi-Pacific plate kinematic model (Fig. 5; Animations 2, 3). The northern Pacific backarc basins are modeled by fragmenting the Izanagi plate during an 85 Ma plate reorganization in the northern Pacific to move the subduction zone offshore following paleomagnetic and magmatic constraints (e.g. Akinin and Miller, 2011; Domeier et al., 2017; Vaes et al., 2019). We do not model Eurasian backarc basins south of Kamchatka due to lack of agreement; instead, we discuss these possibilities in Section 4. We produce a more complete plate reconstruction to the present-day by merging our Izanagi-Pacific plate reconstruction with a published 'tomographic' East Asian plate reconstruction after 52 Ma (Wu et al., 2016).

Izanagi-Pacific plate reconstruction since 120 Ma Fig. 5 shows our unfolded-slab reconstruction since the Early Cretaceous 120 Ma. Note that the leading edge of our reconstructed Izanagi plate (green fill in Fig. 5) is shown with a dashed line to indicate that the plate could be more extensive towards the northwest. This is because our reconstructed Izanagi plate only includes the mid-ocean ridge basalt (MORB) crust formed at the Izanagi-Pacific spreading ridge (i.e. a minimum-size estimate). It is possible the Izanagi plate leading edge also included older Panthalassan Ocean crust that was rifted apart during initial Izanagi-Pacific spreading (e.g. Ueda and Miyashita, 2005); therefore, we do not emphasize our predictions for the start of Izanagi subduction along Eurasia. In contrast, the lateral edges of our reconstructed Izanagi plate are more tightly constrained by the slab unfolding, particularly the SW Izanagi margin, and are tested by magmatism in Section 4. Animations 2 and 3 show the birth of the Pacific triangle within the central Pacific at 190 Ma and progressive spreading of the Izanagi and Pacific rift flanks.

At 120 Ma, the Pacific triangle is located within central Pacific-Panthalassa (Fig. 5a) and the Izanagi-Pacific ridge is actively spreading (Fig. 5a). The SW and NE lateral edges of the Izanagi plate are bounded by transform-like plate boundaries within the central Pacific (Fig. 5a). By 100 Ma, the Izanagi MORB crust formed by Izanagi-Pacific spreading reaches eastern Eurasia and begins to subduct under NE Japan and Sikhote-Alin (Fig. 5b; Animations 2,3). By the late Cretaceous (~85 Ma), the entire width of the Izanagi plate subducts along Eurasia between Korea and northern Russia (Fig. 5c; Animations 2,3). The Izanagi plate is laterally bounded by transform faults; we call the SW transform the 'Qingdao line' because it intersects Eurasia near present Qingdao, China (Fig. 5b, c). Our reconstruction method does not provide enough detail to reconstruct the Qingdao line as a transform fault *sensu* stricto and it might be instead a long-offset, 'leaky' transform fault with small ridge segments (e.g. Lodolo et al., 2013). The northernmost Izanagi plate subducts under the north Pacific backarc basins offshore of northeast Eurasia and Alaska (Fig. 5c). The subduction polarity of the north Pacific backarc basins is uncertain; we reconstruct north-

dipping subduction here but other studies have also reconstructed south-dipping subduction (Domeier et al., 2017; Vaes et al., 2019). The transform fault bounding the northern Izanagi plate intersects and subducts under the northern Pacific backarc basins at ~85 Ma (Fig. 5c; Animations).

At 55 Ma the Izanagi-Pacific ridge intersects Eurasia at a low angle between SW Japan/Korea and Kamchatka (Fig. 5d). Following the global model, westward Pacific plate motions after ~50 Ma initiates subduction along the Qingdao line transform to form the Izu-Bonin-Marianas intra-oceanic subduction zone (Fig. 5e; Animations 2,3). The ~50 Ma subduction initiation ruptures a <3000 km-length of the Qingdao line transform between Bohai Bay-Yellow Sea and the Philippine Sea plate, linking the tectonics of the two distant areas. After 45 Ma, the western Pacific subduction zone that formed along the Qingdao line is progressively overridden by the Philippine Sea plate as it moves northwards from the equator to its present location (Animations 2,3).

4. Discussion

4.1. Comparison to East Asian magmatism and geochemistry

We test our tomographic Izanagi-NW Pacific plate tectonic reconstruction (Fig. 5) against a wide swath (~4500 km) of relatively independent Eurasian continental magmatism along China, Japan, Korea and Sikhote-Alin, Russian Far East (Fig. 6). One testable feature is our reconstructed southern limit of Izanagi subduction along eastern Eurasia between mid-Cretaceous and early Cenozoic times along the 'Qingdao line' sinistral transform (Figs. 5, 6e), which segments Izanagi from another subduction realm to the south that we tentatively call 'South China' (Fig. 5, 6e). Our maximum and minimum case models indicate the Qingdao line intersected Eurasia between ~30°N near present Hangzhou, China, and ~35°N near the southern Korean peninsula (Figs. S6b to d); our preferred 'mean case' location is near the Bohai Bay-Yellow Sea area, China (Figs. 5, 6e).

Eurasian magmatism from the mid-Cretaceous to present shows a stark contrast across our predicted Qingdao line (Fig. 6a to d). Areas north of the Qingdao line show abundant magmatism with enriched isotopic signatures after ~110 Ma that is interrupted by a 56 Ma to 46 Ma magmatic gap, followed by another period of magmatism after 46 Ma (Fig. 6a, b). These observations fit with our modeled Izanagi-Pacific realm in terms of continuous Izanagi subduction since ~100 Ma, a 50 ± 10 Ma Izanagi-Pacific ridge subduction, and, Pacific subduction after ~50 Ma (Fig. 5). In contrast, southeast China magmatism south of the Qingdao line terminates around ~80 Ma to 70 Ma (Figs. 6c, d) and does not resemble magmatism north of our modeled Qingdao line. Other evidence shows the southeast China magmatic arcs spatially advanced towards the Chinese coast between 145 Ma and 90 Ma (Li et al., 2014). These arc migration patterns do not continue north of the Qingdao line, which further supports our inference that southeast China was separate from the Izanagi realm. We do not include NE China and eastern North China igneous rocks in our Fig. 6 analysis because of younger deformation and subsidence around Bohai Bay-Yellow Sea; however, most igneous rocks in these areas are older than mid-Cretaceous (youngest ~73 Ma) (e.g. Wang et al., 2019), which fits with south China magmatism (Fig. 6c,d). Further south, magmatism within SE Asia terminates around 80 Ma to 70 Ma (e.g. Hennig et al., 2017) similar to southeast China (Fig. 6c,d). Therefore, on the basis of our unfolded-slab plate model and relatively independent magmatism, we interpret that SE Asia and southeast China have not resided within the Izanagi realm since the mid-Cretaceous ~100 Ma. Instead, these areas may belong to a separate 'junction' subduction realm between Tethys and Panthalassa (see 4.4.1).

4.2. 50 ± 10 Ma low-angle Izanagi-Pacific ridge-trench intersection with Eurasia

Our tomographic plate model generally affirms previous studies that show a low-angle Izanagi-Pacific ridge-trench intersection with Eurasia in the early Cenozoic (Figs. 4c and 5d). However, in contrast to previous models (Fig. 1c), we limit the ridge subduction to a smaller area between Kamchatka, Sikhote-Alin, Russia, Japan and southernmost Korea (Fig. 5d). Our various cases indicate the Izanagi-Pacific ridge-trench intersection south limit was between present southern Korea to Hangzhou, eastern China (Figs. S6b to d); indeed, we are not aware of any geological evidence for ridge-trench intersection south of these areas during the early Cenozoic. The northern limit of Izanagi-Pacific ridge-trench intersection along Kamchatka is difficult to fully evaluate because the ridge-trench intersection likely occurred along now-vanished north Pacific backarc basins (Fig. 5d) (Konstantinovskaia, 2001; Domeier et al., 2017; Vaes et al., 2019). Our preferred timing for the Izanagi-Pacific ridge-trench intersection is 50±10 Ma (Fig. 4b). Although this timing generally fits with regional magmatism (Fig. 6a, b), the specific Izanagi-Pacific ridge-transform offsets in our plate model (Fig. 5) are extrapolated from the present Pacific plate and not specifically resolved by our reconstruction method. Such variations could explain slightly older or younger ridge-trench intersection ages in localized regions (e.g. 46 to 37 Ma within the Hidaka belt, Japan; Yamasaki et al., 2021).

Our modeled Pacific-Izanagi ridge-trench intersection with Eurasia (Fig. 5) and the magmatic evidence (Fig. 6) challenges previous studies that reconstruct backarc basins along Japan and Sikhote-Alin during the early Cenozoic (e.g. Domeier et al., 2017; Itoh et al., 2017). If such backarc basins existed, they would have precluded tectonic interaction between the Pacific plate and Eurasian continent, similar to the role of the Philippine Sea plate between the Pacific and Eurasia today (e.g. Fig. 1a). For earlier times, it is possible that backarc basins existed along Japan and Sikhote-Alin but were closed and subducted by ~100 to 85 Ma (Ueda and Miyashita, 2005; Boschman et al., 2021). Previously, high heat flow and metamorphism within the Sanbagawa belt around this period (mid- to Late Cretaceous) was explained by Izanagi-Pacific ridge-trench intersection (Maruyama et al., 1997) but this is now incompatible with our results. Instead, future studies should investigate whether accretion or subduction of an intra-oceanic arc during final closure of a backarc basin could account for Sanbagawa belt tectonics during the Cretaceous (Wu et al., 2022).

Evidence from predicted and imaged mantle structure under East Asia

Forward geodynamic models show that low-angle Izanagi-Pacific ridge-trench intersection along Eurasia between 60 Ma to 50 Ma may produce a recognizable, slow-velocity tomographic 'slab gap' between the shallower Pacific and deeper Izanagi slabs (Seton et al., 2015). The ridge subduction slab gap was shown in three tomographic cross-sections between southern Japan and Sikhote-Alin (Seton et al., 2015), which are within our modeled Izanagi-Pacific subduction realm; however, the full extent of the tomographic slab gap is unknown and is further examined here. We first test whether a ridge subduction slab gap is reproducible in a forward geodynamic model with updated plate reconstruction parameters. We assimilate the updated East Asian plate reconstruction (Zahirovic et al., 2014) with corrected Pacific-Panthalassa angular velocities (Torsvik et al., 2019) within a new forward geodynamic model (Figs. 7a and S8; Supplemental Text S2). We find that a higher temperature slab gap is still produced by the Izanagi-Pacific ridge subduction (Figs. 7a and S8). The slab gap shows similarities to co-located global tomographic sections (Figs. 7b, S9).

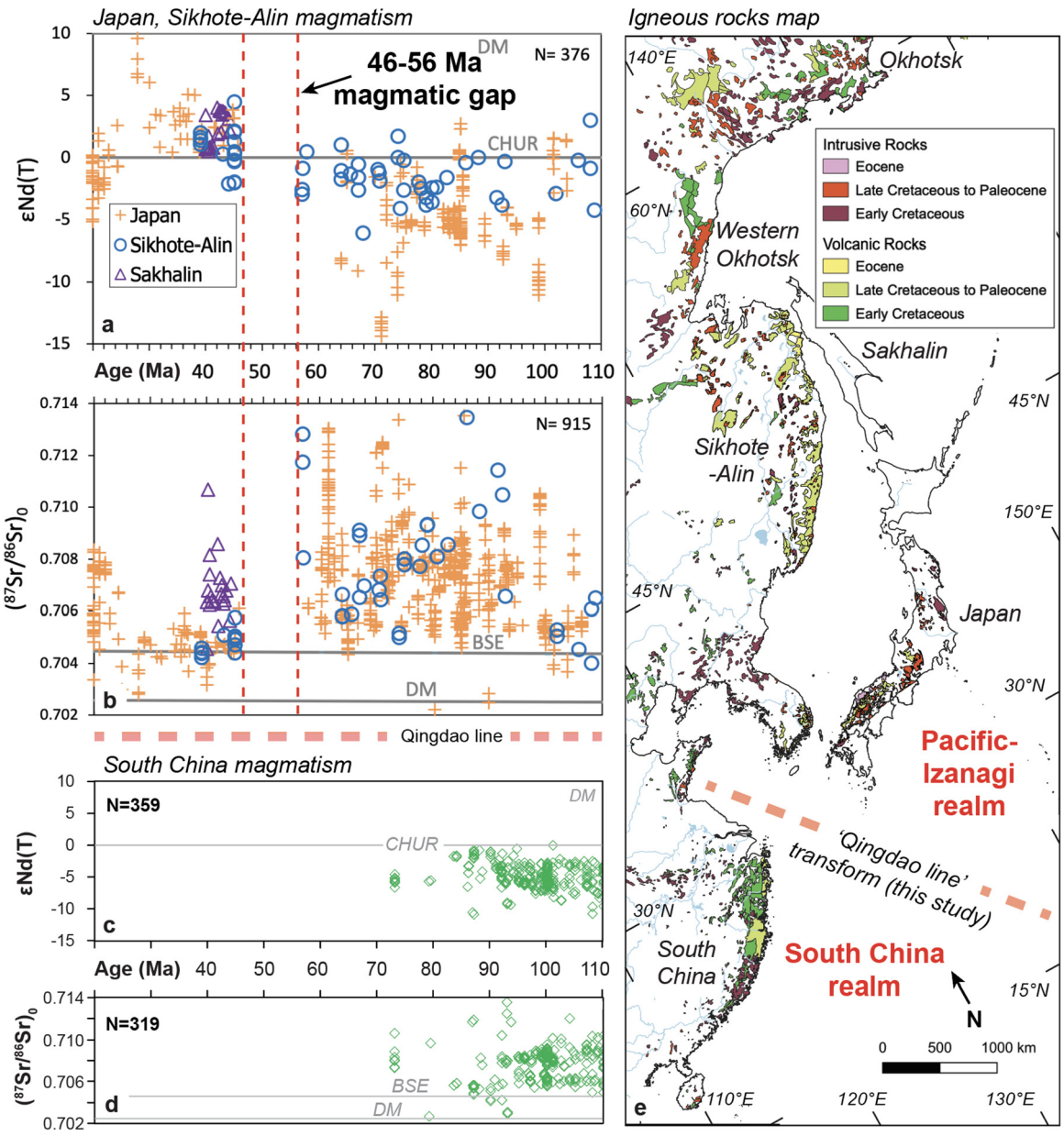

Fig. 6. Compilation of Cretaceous to Miocene intermediate to felsic igneous rocks along the East Asia Eurasian continental margin (see supplementary text for references). a) and b) show Japan and Sikhote-Alin, Russian Far East, igneous ages and neodymium and strontium isotopic values, respectively, north of the reconstructed 'Qingdao line'. c) and d) show south China ages and isotopic values south of the Qingdao line. e) shows a location map of the magmatism and reconstructed 'Qingdao line' from this study. The magmatism shows abrupt contrasts across the Qingdao line. South China magmatism in c) d) ceases after ~75 Ma. In contrast, Japan and Sikhote-Alin magmatism is relatively continuous from 110 to 40 Ma, with the exception of a clear 56 Ma to 46 Ma magmatic gap. The regional geology along Japan and Sikhote-Alin during the 56 to 46 Ma magmatic gap is consistent with our predicted 50 ± 10 Ma Izanagi-Pacific ridge subduction (Wu and Wu, 2019; Kimura et al., 2019).

We build on our slab mapping results and extend our mapped western Pacific mid-slab surface (Fig. 3) deeper into the mantle, mapping across the tomographic slab gap and the deeper Izanagi slabs (e.g. dashed orange line in Fig. 7b). Similar to our earlier western Pacific slab maps (Fig. 3b), we extract mid-slab tomographic velocities and display them on our composite Pacific-Izanagi mid-slab surface (Figs. 7c, d). Our mapping reveals the predicted and imaged tomographic slab gap (Figs. 7a,b) is a through-going feature that can be traced across 4000 km of the East Asian lower mantle primarily between 1000±250 km depths (Figs. 7c, d). The slab gap can be observed in other global tomographic models (Fig. S10). A preliminary slab unfolding of the Izanagi slabs along a single transect under the Russian Far East shows ~7600 km of subducted Izanagi slabs (Fig. S11), which is comparable to our plate model predictions (i.e. ~8100 km of Izanagi slabs subducted between 105 and 55 Ma; Animation 2). These mantle structure observations provide additional evidence for a 50±10 Ma Izanagi-Pacific ridge-trench intersection with eastern Eurasia, which is a key distinguishing feature between many published Izanagi-Pacific plate models (Figs. 1c-e).

4.3. Implications for Izu-Bonin-Marianas (IBM) subduction initiation and the Bohai Bay basin, China

In our models, counter-clockwise rotation of the Pacific plate between ~50 Ma and ~42 Ma (Sharp and Clague, 2006) initiates intra-oceanic subduction along the Qingdao line to form the Izu-Bonin-Marianas (IBM) arcs (Figs. 5d, e). We model the subduction of 60 to 97 Myr old Pacific seafloor (i.e. formed at 110 to 137 Ma) under the Philippine Sea plate during IBM subduction initia-

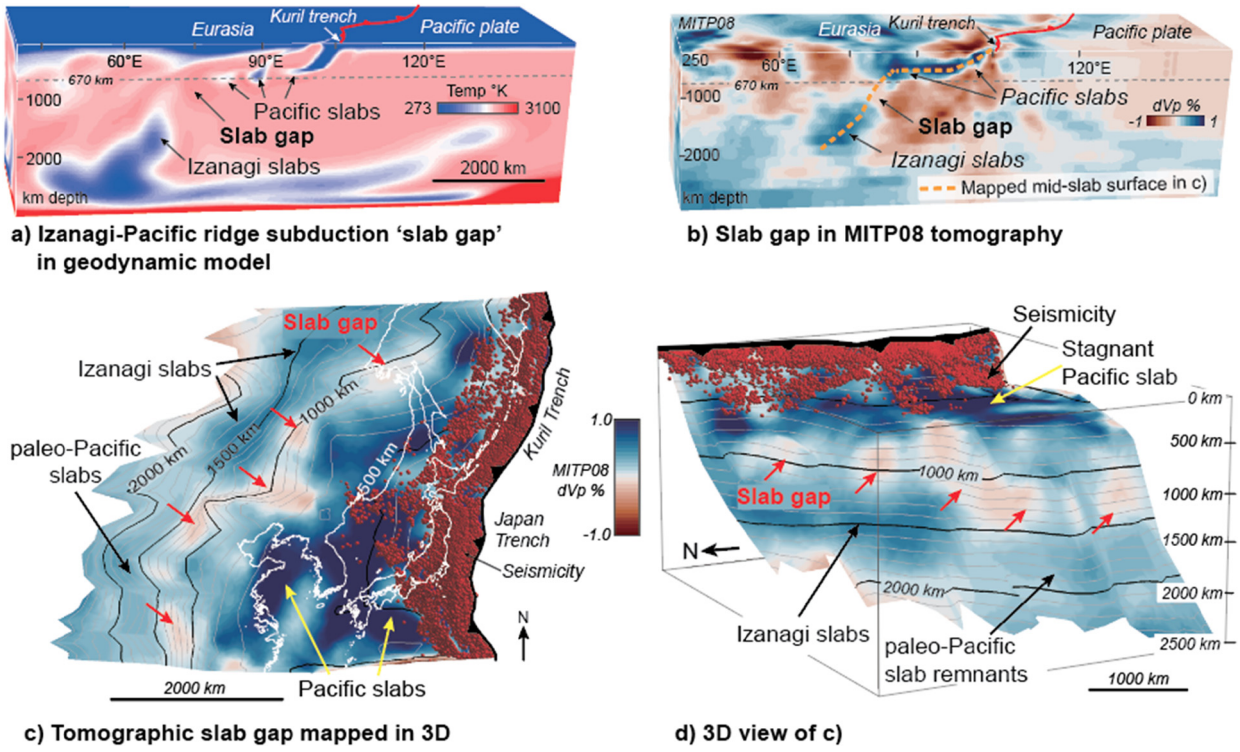

Fig. 7. Predicted and imaged mantle structure showing a ridge subduction 'slab gap' between the Izanagi and Pacific slabs under East Asia. a) 3D visualization of predicted present-day temperature field from a global mantle flow model that used a significantly updated plate model for East Asia (Zahirovic et al., 2014) and Pacific-Panthalassa corrected model 'R' (Torsvik et al., 2019) as boundary conditions. Low angle Izanagi-Pacific ridge-trench intersection between 60 Ma and 50 Ma produced a higher temperature 'slab gap' between the Izanagi and Pacific slabs at 1100 km to 1300 km depth below 75°E. Cross-section location shown by dashed line X-X' in Fig. 1a. b) A co-located MITP08 P-wave tomographic cross-section shows a slab gap between the Pacific and Izanagi slabs that shows similarities to a). c) 3D mapped surface based on the orange dashed line in b) showing extracted mid-slab tomographic velocities across the Pacific slabs, the slab gap, and the Izanagi slabs under East Asia. The map reveals the slab gap in b) is a throughgoing feature that spans across ~4000 km of the mantle under East Asia. d) 3D visualization of the mapped surface in c).

tion (Fig. 5e). Our model indicates that IBM subduction initiation occurred along a former transform, which is generally consistent with IBM models (e.g. Li et al., 2019a). We now reconstruct the former transform as the Qingdao line (Fig. 5d). In addition, the Qingdao line newly links IBM subduction initiation and Eocene tectonic events along the Eurasian margin near Bohai Bay, China (Fig. 5d,e), where it is well-known that basin fault systems abruptly reorganizated around ~42 Ma (e.g. Mao et al., 2019). A link to western Pacific plate tectonics have been speculatively proposed by past studies (e.g. Mao et al., 2019) and are now affirmed by our modeling.

4.4. Implications for adjacent plates in the Mesozoic within eastern Tethys and northwestern Panthalassa

4.4.1. Junction realm

Some global tectonic reconstructions require that a now-vanished plate, or plates, once occupied the junction between Pacific-Panthalassa Ocean and the eastern Tethys Ocean during the Cretaceous (Seton and Müller, 2008; Seton et al., 2012). Provisionally named the 'Junction realm', this location has remained enigmatic because the associated oceanic crust is mostly subducted (Seton and Müller, 2008). Our plate model now shows that subduction along southeast China and northern SE Asia occurred within an unnamed realm that we called 'South China' Fig. 6e). These areas had been previously attributed to the Izanagi realm (Fig. 1c) (Seton and Müller, 2008) but are now excluded from Izanagi by our results; instead, the realm we called 'South China' could be the northern Junction (Fig. 8). By extending Junction northwards to the Qingdao line (i.e. near Bohai Bay-Yellow Sea) during the Cretaceous, our results show the enigmatic Junction realm could be larger than previously recognized (Seton and Müller, 2008). The Junction realm may have included multiple intra-oceanic subduction zones based on the reconstructed Pontus Ocean (van der Meer et al., 2012).

4.4.2. Early Pacific plate growth

Our models suggest that the Qingdao line transform fault became the transition between Junction and the Izanagi-Pacific realm by late Cretaceous times (Fig. 8b) and possibly earlier (Fig. 8a). The early growth of the Pacific plate in the early Jurassic has been modeled from a ridge-ridge-ridge triple junction (i.e. Pacific triangle) that had three sinistral transform faults radiating from the ridge vertices (Boschman and van Hinsbergen, 2016). Our Qingdao line sinistral transform bears likeness to the Izanagi-Phoenix transform in these models (Fig. 8a) (Boschman and van Hinsbergen, 2016). This suggests that the Qingdao line is a remnant feature from the early birth of the Pacific plate that eventually reached the Eurasian margin near East Asia (Fig. 8b).

4.4.3. Kula plate

Our modeled Izanagi realm limits the western extent of the Kula plate near the longitude of northern Russia-westernmost Alaska during Late Cretaceous times (Fig. 5c,d); uncertainties in our slab unfolding (Fig. S7b) could place the Kula-Izanagi boundary as far westwards as present Okhotsk, Russia. In either case, our plate modeling indicates that the Kula plate was a relatively small plate located within the northern Pacific (Fig. 8b) that never subducted near East Asia during Cretaceous or early Cenozoic times, in contrast to previous models (Lewis et al., 2002; Engebretson et al., 1985). Instead, our modeled Kula plate boundary is most consistent with plate models previously proposed by Müller et al. (2016) (Fig. 1c). Taken together, the new divisions between the Izanagi, Kula and Junction realms revealed by our tomographic plate model (compare Figs. 1c-e and 8) now reveal a more complex, segmented

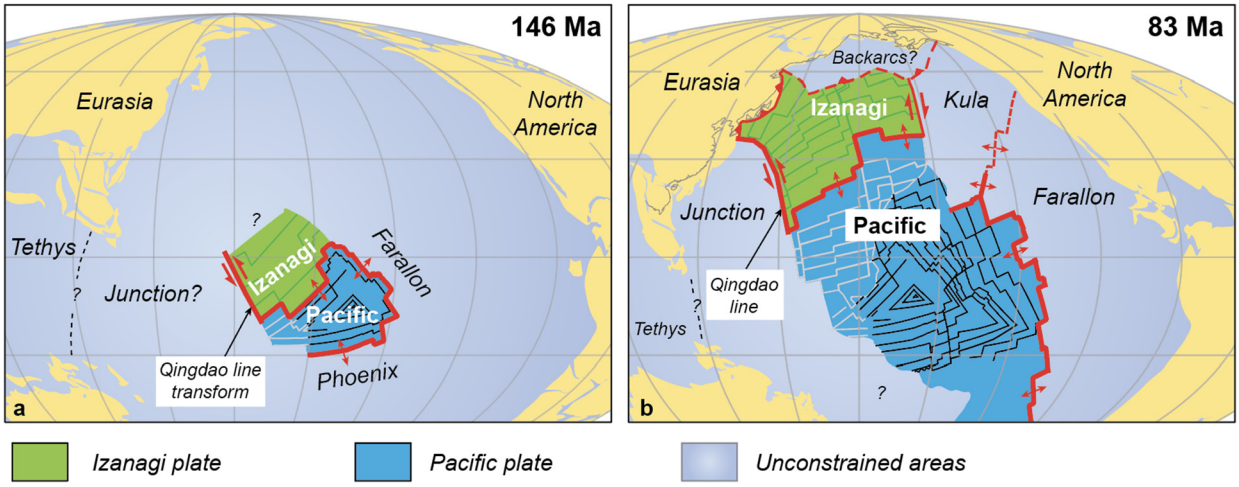

Fig. 8. Pacific-Panthalassa plate tectonics since Cretaceous times based on the results from this study. a) At the latest Jurassic, early growth of the Pacific plate was accommodated by a sinistral transform along the southwestern Izanagi plate margin (the Qingdao line). b) During late Cretaceous times, the Izanagi plate subducted along the Eurasian continental margin north of the Qingdao line. Subduction south of the Qingdao line occurred along South China and SE Asia within a separate realm that we link to the poorly-known plate tectonic 'Junction' between Pacific-Panthalassa and Tethys. The western Kula plate was limited to the NW Cordillera of North America and did not extend into East Asia. Synthetic seafloor isochrons and the global plate model are modified from Matthews et al. (2016). Absolute plate positions are based on the 'Model R' corrected Panthalassa mantle reference of Torsvik et al. (2019). North Pacific backarc basins follow previous studies (Vaes et al., 2019; Domeier et al., 2017). Gray lines within the Pacific plate show modeled regions; black lines show existing regions.

NW Pacific-Panthalassa superocean during Pangea supercontinent breakup than previously recognized.

5. Conclusions

The Pacific-Panthalassa realm is traditionally modeled as a four-plate system formed by the Pacific plate and its three conjugates: the Izanagi, Farallon and Phoenix plates (Seton et al., 2012; Matthews et al., 2016; Müller et al., 2016). We present a fully-kinematic NW Pacific-Izanagi plate model from tomographically-imaged western Pacific mantle structure that implies the Izanagi plate subducted along eastern Eurasia between present northern Russia and Bohai Bay-Yellow Sea, China, during the mid-Cretaceous to early Cenozoic. The southwest margin of the Izanagi plate was a transform-style plate boundary that intersected Eurasia near present Qingdao, China, during the Late Cretaceous, and possibly earlier. This previously unrecognized plate boundary, which we name the 'Qingdao line', explains the abrupt change in continental arc magmatism between northeast China and southeast China during the Cretaceous. Our model confirms a low-angle Izanagi-Pacific ridge-trench intersection with Eurasia at 50 $\pm$ 10 Ma but limits the ridge subduction between Korea, Japan and the Russian Far East. The Kula plate was a small plate within the northern Pacific basin and never subducted along the East Asia Eurasian margin. We exclude South China and southeast Asia from Pacific-Panthalassa during the Cretaceous; instead, these areas were within the enigmatic plate tectonic 'Junction' between Pacific-Panthalassa and Tethys. Future study of the lower half of the East Asian mantle, which was not considered here, may further reveal earlier plate tectonic details of Panthalassa and Junction during our most recent supercontinent breakup and superocean demise.

CRediT authorship contribution statement

Jonny Wu: Conceptualization, Investigation, Methodology, Supervision, Visualization, Writing – original draft. **Yi-An Lin:** Investigation, Visualization. **Nicolas Flament:** Conceptualization, Investigation, Writing – original draft. **Jeremy Tsung-Jui Wu:** Investigation, Visualization. **Yiduo Liu:** Investigation, Visualization.

Declaration of competing interest

The authors declare that they have no known competing financial interests or personal relationships that could have appeared to influence the work reported in this paper.

Acknowledgements

Jonny Wu, Yi-An Lin, and Tsung-Jui Wu were supported by US National Science Foundation grant EAR-1848327. Jonny Wu, Yi-An Lin, Tsung-Jui Wu and Yiduo Liu were also supported by a Texas Governor's University Research Initiative (GURI) award to John Suppe. Nicolas Flament was supported by ARC grants DE160101020 and LP170100863. Maria Seton is thanked for providing plate tectonic expertise, published GPlates synthetic seafloor isochrons and other Pacific-Panthalassa plate reconstruction constraints. Lorenzo Colli, John Suppe, Spencer Fuston, Yi-Wei Chen, Gaku Kimura, Hayato Ueda, Kazu Okamoto, Ying Song, Xi Xu, Yin Liu, Lydian Boschman, Douwe van Hinsbergen, Bram Vaes, Steve Grand, Mark Hoggard, Julia Ribeiro and Daniel Woodworth are thanked for helpful scientific discussions. Emerson Paradigm provided GOCAD educational licenses to the University of Houston, Texas. GPlates free software from the Earthbyte Group was used for the plate reconstructions. Scientific Color Maps from Fabio Crameri were used to plot tomography color scales. The northwest Pacific-Izanagi plate model presented here are included as digital GPlates files and as three Movie Animations in the Supplementary Material. Grace Shephard, Andrew Parsons and Editors An Yin and Alexander Webb are thanked for constructive and thorough reviews.

Appendix A. Supplementary material

Supplementary material related to this article can be found online at https://doi.org/10.1016/j.epsl.2022.117445.

References

Akinin, V.V., Miller, E.L., 2011. Evolution of calc-alkaline magmas of the Okhotsk-Chukotka volcanic belt. Petrology 19, 237–277.

Boschman, L.M., van Hinsbergen, D.J.J., Spakman, W., 2021. Reconstructing Jurassic-Cretaceous intra-oceanic subduction evolution in the northwestern Panthalassa Ocean using ocean plate stratigraphy from Hokkaido, Japan. Tectonics 40, e2019TC005673.

Boschman, L.M., van Hinsbergen, D.J.J., 2016. On the enigmatic birth of the Pacific Plate within the Panthalassa Ocean. Sci. Adv. 2.

Čížková, H., Bina, C.R., 2013. Effects of mantle and subduction-interface rheologies on slab stagnation and trench rollback. Earth Planet. Sci. Lett. 379, 95–103.

Cooper, A.K., Scholl, D.W., Marlow, M.S., 1976. Plate tectonic model for the evolution of the eastern Bering Sea basin. GSA Bull. 87, 1119–1126.

Domeier, M., Shephard, G.E., Jakob, J., Gaina, C., Doubrovine, P.V., Torsvik, T.H., 2017. Intraoceanic subduction spanned the Pacific in the Late Cretaceous–Paleocene. Sci. Adv. 3.

Dziewonski, A.M., Anderson, D.L., 1981. Preliminary reference Earth model. Phys. Earth Planet. Inter. 25, 297–356.

Engebretson, D.C., Cox, A., Gordon, R.G., 1985. Relative motions between oceanic and continental plates in the Pacific basin. In: Engebretson, D.C., Cox, A., Gordon, R.G. (Eds.), Relative Motions Between Oceanic and Continental Plates in the Pacific Basin. Geological Society of America.

Fuston, S., Wu, J., 2020. Raising the Resurrection plate from an unfolded-slab plate tectonic reconstruction of northwestern North America since early Cenozoic time. Geol. Soc. Am. Bull. 133, 1128–1140.

Grebennikov, A.V., Kemkin, I.V., Khanchuk, A.I., 2021. Paleocene–early Eocene post-subduction magmatism in Sikhote-Alin (Far East Russia): new constraints for the tectonic history of the Izanagi-Pacific ridge and the East Asian continental margin. Geosci. Front. 12, 101142.

Hennig, J., Breitfeld, H.T., Hall, R., Nugraha, A.M.S., 2017. The Mesozoic tectono-magmatic evolution at the Paleo-Pacific subduction zone in West Borneo. Gondwana Res. 48, 292–310.

Itoh, Y., Takano, O., Takashima, R., 2017. Tectonic Synthesis: A Plate Reconstruction Model of the NW Pacific Region Since 100 Ma.

Jaxybulatov, K., Koulakov, I., Dobretsov, N.L., 2013. Segmentation of the Izu-Bonin and Mariana slabs based on the analysis of the Benioff seismicity distribution and regional tomography results. Solid Earth 4, 59–73.

Kimura, G., Kitamura, Y., Yamaguchi, A., Kameda, J., Hashimoto, Y., Hamahashi, M., 2019. Origin of the early Cenozoic belt boundary thrust and Izanagi–Pacific ridge subduction in the western Pacific margin. Isl. Arc 28, e12320.

Konstantinovskaia, E.A., 2001. Arc–continent collision and subduction reversal in the Cenozoic evolution of the Northwest Pacific: an example from Kamchatka (NE Russia). Tectonophysics 333, 75–94.

Kutyrev, A.V., Kamenetsky, V.S., Park, J.-W., Maas, R., Demonterova, E.I., Antsiferova, T.N., Ivanov, A.V., Hwang, J., Abersteiner, A., Ozerov, A.Y., 2021. Primitive high-K intraoceanic arc magmas of Eastern Kamchatka: Implications for Paleo-Pacific tectonics and magmatism in the Cretaceous. Earth-Sci. Rev. 220, 103703.

Lewis, J.C., Byrne, T.B., Tang, X., 2002. A geologic test of the Kula-Pacific Ridge capture mechanism for the formation of the West Philippine Basin. GSA Bull. 114, 656–664.

Li, C., van der Hilst, R.D., Engdahl, E.R., Burdick, S., 2008. A new global model for P wave speed variations in Earth's mantle. Geochem. Geophys. Geosyst. 9, Q05018.

Li, C., 2007. Evolution of upper mantle beneath East Asia and the Tibetan Plateau from P-wave tomography. Ph.D thesis. Massachusetts Institute of Technology. 196 pp.

Li, H.-Y., Taylor, R.N., Prytulak, J., Kirchenbaur, M., Shervais, J.W., Ryan, J.G., Godard, M., Reagan, M.K., Pearce, J.A., 2019a. Radiogenic isotopes document the start of subduction in the Western Pacific. Earth Planet. Sci. Lett. 518, 197–210.

Li, J., Zhang, Y., Dong, S., Johnston, S.T., 2014. Cretaceous tectonic evolution of South China: a preliminary synthesis. Earth-Sci. Rev. 134, 98–136.

Li, Z.X., Mitchell, R.N., Spencer, C.J., Ernst, R., Pisarevsky, S., Kirscher, U., Murphy, J.B., 2019c. Decoding Earth's rhythms: modulation of supercontinent cycles by longer superocean episodes. Precambrian Res. 323, 1–5.

Liu, X., Zhao, D., Li, S., Wei, W., 2017. Age of the subducting Pacific slab beneath East Asia and its geodynamic implications. Earth Planet. Sci. Lett. 464, 166–174.

Lodolo, E., Coren, F., Ben-Avraham, Z., 2013. How do long-offset oceanic transforms adapt to plate motion changes? The example of the Western Pacific-Antarctic plate boundary. J. Geophys. Res., Solid Earth 118, 1195–1202.

Lonsdale, P., 1988. Paleogene history of the Kula plate: offshore evidence and onshore implications. GSA Bull. 100, 733–754.

Mao, L., Tian, J., Wang, L., Zhang, C., Zhang, W., Tian, R., Wang, X., Ming, J., Xiao, A., 2019. Initiation and origin of dextral deformation at Mid-Eocene in the western Bohai Bay Basin, East China. J. Asian Earth Sci. 185, 104031.

Maruyama, S., Isozaki, Y., Kimura, G., Terabayashi, M., 1997. Paleogeographic maps of the Japanese Islands: Plate tectonic synthesis from 750 Ma to the present. Isl. Arc 6, 121–142.

Matthews, K.J., Maloney, K.T., Zahirovic, S., Williams, S.E., Seton, M., Müller, R.D., 2016. Global plate boundary evolution and kinematics since the late Paleozoic. Glob. Planet. Change 146, 226–250.

Miller, M.S., Kennett, B.L.N., Toy, V.G., 2006. Spatial and temporal evolution of the subducting Pacific plate structure along the western Pacific margin. J. Geophys. Res., Solid Earth 111, B02401.

Mitchell, R.N., Thissen, C.J., Evans, D.A.D., Slotznick, S.P., Coccioni, R., Yamazaki, T., Kirschvink, J.L., 2021. A Late Cretaceous true polar wander oscillation. Nat. Commun. 12, 3629.

Müller, R.D., Seton, M., Zahirovic, S., Williams, S.E., Matthews, K.J., Wright, N.M., Shephard, G.E., Maloney, K.T., Barnett-Moore, N., Hosseinpour, M., Bower, D.J., Cannon, J., 2016. Ocean basin evolution and global-scale plate reorganization events since Pangea breakup. Annu. Rev. Earth Planet. Sci. 44, 107–138.

Müller, R.D., Cannon, J., Qin, X., Watson, R.J., Gurnis, M., Williams, S., Pfaffelmoser, T., Seton, M., Russell, S.H.J., Zahirovic, S., 2018. GPlates: building a virtual Earth through deep time. Geochem. Geophys. Geosyst. 19, 2243–2261.

Nakanishi, M., Tamaki, K., Kobayashi, K., 1989. Mesozoic magnetic anomaly lineations and seafloor spreading history of the northwestern Pacific. J. Geophys. Res., Solid Earth 94, 15437–15462.

Osozawa, S., Usuki, T., Usuki, M., Wakabayashi, J., Jahn, B.-m., 2019. Trace elemental and Sr-Nd-Hf isotopic compositions, and U-Pb ages for the Kitakami adakitic plutons: insights into interactions with the early Cretaceous TRT triple junction offshore Japan. J. Asian Earth Sci. 103968.

Parsons, A.J., Sigloch, K., Hosseini, K., 2021. Australian Plate Subduction is Responsible for Northward Motion of the India-Asia Collision Zone and ~1,000 km Lateral Migration of the Indian Slab. Geophysical Research Letters 48, e2021GL094904.

Richards, F.D., Hoggard, M.J., Cowton, L.R., White, N.J., 2018. Reassessing the thermal structure of oceanic lithosphere with revised global inventories of basement depths and heat flow measurements. J. Geophys. Res., Solid Earth 123, 9136–9161.

Seton, M., Flament, N., Whittaker, J., Müller, R.D., Gurnis, M., Bower, D.J., 2015. Ridge subduction sparked reorganization of the Pacific plate-mantle system 60–50 million years ago. Geophys. Res. Lett. 42, 1732–1740.

Seton, M., Müller, D., 2008. Reconstructing the junction between Panthalassa and Tethys since the Early Cretaceous. In: Eastern Australasian Basins III. Petroleum Exploration Society of Australia. Special Publications, pp. 263–266.

Seton, M., Müller, R.D., Zahirovic, S., Gaina, C., Torsvik, T., Shephard, G., Talsma, A., Gurnis, M., Turner, M., Maus, S., Chandler, M., 2012. Global continental and ocean basin reconstructions since 200 Ma. Earth-Sci. Rev. 113, 212–270.

Shephard, G.E., Matthews, K.J., Hosseini, K., Domeier, M., 2017. On the consistency of seismically imaged lower mantle slabs. Sci. Rep. 7, 10976.

Simmons, N.A., Schuberth, B.S.A., Myers, S.C., Knapp, D.R., 2019. Resolution and covariance of the LLNL-G3D-JPS global seismic tomography model: applications to travel time uncertainty and tomographic filtering of geodynamic models. Geophys. J. Int. 217, 1543–1557.

Sharp, W.D., Clague, D.A., 2006. 50-Ma initiation of Hawaiian-Emperor bend records major change in Pacific plate motion. Science 313, 1281–1284.

Tao, K., Grand, S.P., Niu, F., 2018. Seismic structure of the upper mantle beneath eastern Asia from full waveform seismic tomography. Geochem. Geophys. Geosyst. 19, 2732–2763.

Tang, Y., Obayashi, M., Niu, F., Grand, S., Chen, J., Kawakatsu, H., Tanaka, S., Ning, J., Ni, J., 2014. Changbaishan volcanism in northeast China linked to subduction-induced mantle upwelling. Nat. Geosci. 7, 470–475.

Torsvik, T.H., Steinberger, B., Shephard, G.E., Doubrovine, P.V., Gaina, C., Domeier, M., Conrad, C.P., Sager, W.W., 2019. Pacific-Panthalassic reconstructions: overview, errata and the way forward. Geochem. Geophys. Geosyst. 20, 3659–3689.

Uyeda, S., Miyashiro, A., 1974. Plate tectonics and the Japanese islands: a synthesis. GSA Bull. 85, 1159–1170.

Ueda, H., Miyashita, S., 2005. Tectonic accretion of a subducted intraoceanic remnant arc in Cretaceous Hokkaido, Japan, and implications for evolution of the Pacific northwest. Isl. Arc 14, 582–598.

Vaes, B., van Hinsbergen, D.J.J., Boschman, L.M., 2019. Reconstruction of subduction and back-arc spreading in the NW Pacific and Aleutian basin: clues to causes of Cretaceous and Eocene plate reorganizations. Tectonics 38, 1367–1413.

van der Hilst, R., Seno, T., 1993. Effects of relative plate motion on the deep structure and penetration depth of slabs below the Izu-Bonin and Mariana island arcs. Earth Planet. Sci. Lett. 120, 395–407.

van der Meer, D.G., Torsvik, T.H., Spakman, W., van Hinsbergen, D.J.J., Amaru, M.L., 2012. Intra-Panthalassa Ocean subduction zones revealed by fossil arcs and mantle structure. Nat. Geosci. 5, 215.

Van Der Meer, D.G., Zeebe, R.E., van Hinsbergen, D.J.J., Sluijs, A., Spakman, W., Torsvik, T.H., 2014. Plate tectonic controls on atmospheric CO_2 levels since the Triassic. Proc. Natl. Acad. Sci. USA 111, 4380.

Wang, T., Niu, M.-L., Wu, Q., Li, X.-C., Cai, Q.-R., Zhu, G., 2019. Episodic bimodal magmatism at an active continental margin due to Paleo-Pacific Plate subduction: a case study from the southern segment of the Tan-Lu Fault Zone, eastern China. Lithos 328–329, 159–181.

Whittaker, J.M., Müller, R.D., Leitchenkov, G., Stagg, H., Sdrolias, M., Gaina, C., Goncharov, A., 2007. Major Australian-Antarctic plate reorganization at Hawaiian-Emperor bend time. Science 318, 83–86.

Woods, M.T., Davies, G.F., 1982. Late Cretaceous genesis of the Kula plate. Earth Planet. Sci. Lett. 58, 161–166.

Wu, J., Suppe, J., Lu, R., Kanda, R., 2016. Philippine Sea and East Asian plate tectonics since 52Ma constrained by new subducted slab reconstruction methods. J. Geophys. Res., Solid Earth 121, 4670–4741.

Wu, J.T.-J., Wu, J., 2019. Izanagi-Pacific ridge subduction revealed by a 56 to 46 Ma magmatic gap along the northeast Asian margin. Geology 47, 953–957.
Wu, J.T.-J., Wu, J., Okamoto, K., 2022. Intra-oceanic arc accretion along Northeast Asia during Early Cretaceous provides a plate tectonic context for North China craton destruction. Earth-Sci. Rev. 226, 103952.
Yamasaki, T., Nanayama, F., 2018. Immature intra-oceanic arc-type volcanism on the Izanagi Plate revealed by the geochemistry of the Daimaruyama greenstones in the Hiroo Complex, southern Hidaka Belt, central Hokkaido, Japan. Lithos 302–303, 224–241.
Yamasaki, T., Shimoda, G., Tani, K., Maeda, J., Nanayama, F., 2021. Subduction of the Izanagi-Pacific Ridge–transform intersection at the northeastern end of the Eurasian plate. Geology 49, 952–957.
Zahirovic, S., Seton, M., R.D., Müller, 2014. The Cretaceous and Cenozoic tectonic evolution of Southeast Asia. Solid Earth 5, 227–273.